A Carbon Nanotube-Based Coulter Nanoparticle Counter

TAKASHI ITO, LI SUN,
RONALD R. HENRIQUEZ, AND
RICHARD M. CROOKS*
Department of Chemistry, Texas A&M University,
Post Office Box 30012, College Station, Texas 77842-3012

Received April 26, 2004

ABSTRACT
This Account reports on the properties and applications of carbon nanotube-based Coulter counters (CNCCs). CNCCs provide a means for determining the diameter and electrophoretic mobility (or electrokinetic surface charge) of individual nanoparticles dispersed in aqueous solutions, as well as the nanoparticle concentration. Such measurements do not require CNCC calibration or sample labeling. Because CNCCs measure the characteristics of individual particles, they provide the true average and polydispersity distribution of nanoparticle properties. CNCCs can differentiate between individual nanoparticles based on their surface charge and size, and CNCCs can be used to determine the apparent surface pK_a of polymeric nanoparticles. Nanoparticle characterization by CNCC, electron microscopy, conductometric titration, and light scattering are compared.

Introduction

This Account reports on carbon nanotube-based Coulter counters (CNCCs) and their applications for studying the properties of nanoparticles.[1−3] CNCCs provide a means for determining the size, electrophoretic mobility, and electrokinetic surface charge of individual nanoparticles dispersed in an aqueous solution. CNCCs can also be used to measure the concentration of nanoparticles. All of this information can be determined without calibration, standards, or labeling the sample.[2] CNCCs based on multiwall carbon nanotube (MWNT) channels ranging in diameter from 130 to 150 nm can be used to determine the size of particles having diameters in the 28−100 nm size range. It is not possible to measure such small particles using conventional Coulter counters that have micrometer-scale channels. Moreover, because CNCCs measure the characteristics of individual particles, they provide the true average and polydispersity distribution of nanoparticle properties. Accordingly, CNCCs can be used for differentiating individual nanoparticles based on their surface charge and size, and for determining their apparent surface pK_a values.

Coulter counters consist of two chambers divided by an insulating membrane that contains a single channel (Chart 1a).[4] Electrodes immersed in an electrolyte in each chamber are used to drive an ionic current through the channel. If particles having a size on the order of the channel diameter are present in the electrolyte, then they may be driven into the channel and thereby cause a reduction in ionic current. The output of a Coulter counter is a plot of ionic current versus time (Chart 1b) exhibiting a string of current pulses. Under favorable conditions, these current pulses can be correlated to the size, mobility, and concentration of the particles.

The Coulter counter was patented in 1953 by W. H. Coulter,[4] and throughout the last 50 years, such devices having channels ranging from 10 to 100 μm in diameter have been widely used in biological and medical laboratories to determine biological cell concentrations.[5] During the 1970s, DeBlois and Bean showed for the first time that

Chart 1[a]

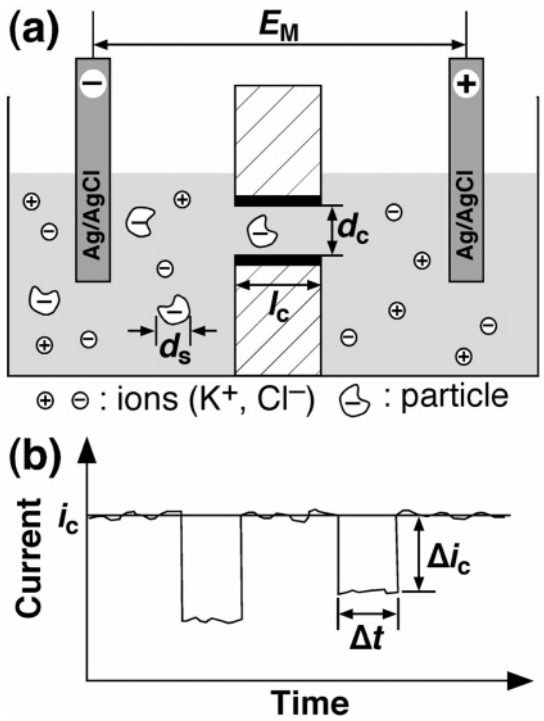

[a] Reproduced with permission from ref 18. Copyright 2004, Royal Society of Chemistry.

Takashi Ito received his B.S., M.S., and Ph.D. degrees in chemistry from the University of Tokyo in 1993, 1995, and 1998, respectively. Subsequently, he worked as a research associate at Tokyo University of Science (1998−2001). He was a postdoctoral research associate at Texas A&M University from 2001 to 2004. He is presently an assistant professor of chemistry at Kansas State University. His research interests include chemical sensors based on nanomaterials and scanning probe microscopy using chemically modified tips.

Li Sun received his undergraduate education at Beijing University and a Ph.D. degree in chemistry from Northwestern University (1990). At present, he is a research scientist at Texas A&M University. His research interests include fluidic transport through nanoporous media and their applications to bioanalysis.

Ronald R. Henriquez received his B.S. degree in chemistry from the University of Texas at Dallas in 2001, and he is currently pursuing his doctoral studies under the guidance of Prof. Richard M. Crooks. His research interests include electrochemistry, nanomaterial-based chemical sensors, and their applications to bioanalysis.

Richard M. Crooks received his B.S. degree in chemistry from the University of Illinois (Urbana, IL) and his doctoral degree in electrochemistry from the University of Texas (Austin, TX) in 1987. He is currently professor of chemistry and chemical engineering and director of the Center for Integrated Microchemical Systems, at Texas A&M University. His research interests include electrochemistry, biosensing, nanomaterials, catalysis, and applications of microfluidic devices.

* To whom correspondence should be addressed. E-mail: crooks@tamu.edu. Telephone: 979-845-5629. Fax: 979-845-1399.

10.1021/ar040108+ CCC: $27.50
Published on Web 10/15/2004

a 450-nm diameter channel fabricated by track etching of a polycarbonate membrane could be used to characterize polystyrene particles as small as 90 nm in diameter.[6] Additionally, they performed pioneering virus-detection experiments using this same approach.[7,8] Although their body of work demonstrated that the Coulter principle could be implemented on the submicrometer scale, almost 2 decades passed before channels smaller than about 0.5 μm were reported. This is largely due to the technical challenge of fabricating and characterizing single, nanometer-scale channels in insulating membranes.

The renewed interest in Coulter counting during the past decade is largely a consequence of recent advances in channel fabrication methods and high-resolution characterization techniques. Smaller more robust channels hold out the promise of reproducibly measuring the properties of analytes on the 1−50 nm size scale. Many interesting analytes, such as organic molecules, hydrated metal ions, viruses, colloids, proteins, nucleic acids, and other natural and synthetic polymers, have sizes in this range. From an analytical perspective, Coulter counters have additional attractive properties. First, the Coulter counting principle has a broad dynamic range that spans at least 6 orders of magnitude, roughly 1 nm to 1 mm. Second, Coulter counters detect analytes one particle at a time; therefore, the method has inherent single-particle sensitivity. Third, Coulter counting requires only that analyte size be comparable to the size of the sensing channel, and therefore no spectroscopic, electrochemical, or enzymatic labeling is required. Finally, from a technology viewpoint, Coulter counters are simple, have low power requirements, and are intrinsically compact (portable).

At present, there are three active research areas related to Coulter counting. The first focuses on new methods for fabricating channels having very small dimensions. Such channels can be constructed either from synthetic materials or from self-assembling membrane proteins. For example, a synthetic (nonbiological) single channel (3−10 nm in diameter) has been milled through a Si_3N_4 membrane using an ion beam and then used for counting 0.5−10 kb, double-stranded DNA (dsDNA).[9,10] Similarly, a single channel having a conical shape with a ∼2−7 nm constriction at the tip was prepared by track etching of a polyimide membrane and used to discriminate between different-length dsDNA.[11] Smaller sensing channels (<2 nm in diameter) were formed using α-hemolysin, a membrane protein confined to a lipid bilayer, to detect individual hydrated metal ions, organic molecules, and single-strand DNA.[12−14] The second area of research involves integration of Coulter counters with microchemical analysis systems. For example, a quartz-based microchip Coulter counter fabricated via electron-beam lithography could be used to detect polymer particles as small as 87 nm in diameter.[15] Channels ranging from 200 to 500 nm in diameter and made of poly(dimethylsiloxane) (PDMS) were prepared via a process that combines elastomer molding and electron-beam lithography, and these were used to detect Lambda-phage DNA[16] and the change in size of streptavidin-coated colloid particles induced by antibody−antigen binding.[17] The third area of research involves chemical modification of the sensing channel to impart chemical selectivity. For example, site-directed mutagenesis in α-hemolysin makes it possible to prepare a protein channel having an interior that selectively binds to Zn^{2+}.[13] Additional information about the present state of research in this field can be found in a recent review.[18]

Operating Principle

The operating principle of Coulter counters is based on the reduction in ionic current associated with transport of an analyte particle through a sensing channel (Chart 1).[19] The pulse height is used to determine particle size; the pulse width can, under favorable conditions, be used to determine the charge carried by the particle; and the frequency of the current pulses is related to particle concentration.

The ratio of the pulse height to the baseline current is roughly the same as the particle volume relative to the channel volume. For a cylindrical channel biased at a constant voltage (E_M, the membrane potential), the relative decrease in current is given by eq 1. Here, i_c is the baseline

$$\frac{\Delta i_c}{i_c} = S(d_c,d_s)\frac{{d_s}^3}{l_c' {d_c}^2} \qquad (1)$$

ionic current, Δi_c is the pulse height, d_s is the diameter of the analyte particle, d_c is the channel diameter, and l_c is the channel length. l_c' is the channel length after correcting for the so-called "end effect" ($l_c' = l_c + 0.785d_c$).[6,20] The correction factor $S(d_c,d_s)$ depends on the diameter ratio, d_c/d_s, and it can be approximated by eq 2 with less than a 2% error if the diameter ratio is less than 0.8.[6]

$$S(d_c,d_s) = \frac{1}{1 - 0.8(d_c/d_s)^3} \qquad (2)$$

Equation 1 shows that the pulse height is a very sensitive (cubic) function of the analyte diameter; thus, a slight change in analyte diameter results in a large change in pulse height.

The pulse width, Δt, is inversely proportional to the analyte velocity, v_s, which is in turn determined by the transport properties of the analyte as it transverses the sensing channel. In the absence of specific chemical interactions between analytes and the channel itself there are four fundamental mechanisms that can potentially contribute to particle transport: pressure-driven flow, electrophoresis, electroosmosis, and diffusion.[1] However, when all four transport modes are operative it is difficult to extract useful analytical information from Δt. This is because the transport modes are interdependent, and therefore, the equations governing the velocity of the analyte are complex.[21] As we will see later, only when a single mode of transport dominates the other three is the situation simplified. This is the case for nanotube-based

Coulter counters, because there is no charge on the interior surface of the channel. It is not possible to make this simplification for other types of Coulter counters, however, because their channels are made of materials such as glass, sapphire, or polycarbonate, all of which display immobile surface charges.

The pulse frequency, J_s, in Coulter counting is related to the velocity and the concentration of the analyte particles C_s (eq 3).[1] Because the average velocity can be

$$J_s = \frac{\pi v_s d_c^2}{4} C_s \qquad (3)$$

determined from the pulse width, the analyte concentration can be determined without calibration using eq 3.[1,2] A more in-depth theoretical treatment of Coulter counting can be found in a recent review.[22]

Characteristics of CNCCs

MWNTs and Device Fabrication. We chose to use MWNTs as the sensing channel for Coulter counting of nanosized particles because of the following four desirable material properties.[4,23] First, MWNTs having diameters ranging from a few nanometers to hundreds of nanometers are commercially available. This size range is suitable for detecting a wide variety of interesting analytes of biochemical significance (vide supra). Second, MWNTs have uniform and precise channel diameters, which is essential for accurate particle sizing. Third, MWNTs have negligible charge on the graphitic inner surface. This means electroosmotic flow is suppressed and that therefore the electrophoretic mobility of the analyte can be easily determined.[1] Fourth, we have developed a microtoming method for producing hundreds of channels having identical diameters from a single MWNT.[1]

Chart 2 shows the methodology for fabricating single-channel membranes using MWNT channels ranging in diameter from 60 to 160 nm.[1,2] An *xyz*-translation stage attached to an optical microscope was used for the manipulations shown in parts a−c of Chart 2. The first step is to remove a single MWNT from a bundle using a sharpened Pt/Ir tip having acrylic adhesive on its apex (Chart 2a).[24,25] Next, one end of the nanotube was capped with electropolymerized polypyrrole (Chart 2b)[25] to prevent ingress of the epoxy used in the next step.[2,25] The MWNT was then immobilized onto a Au TEM grid using Ag epoxy, and transmission electron microscopy (TEM) was used to ensure that the interior was not blocked by epoxy or other substances (Chart 2c). The grid-immobilized MWNT was embedded in an epoxy matrix (Chart 2d), and the resulting epoxy block was microtomed to yield small sections (ca. 1 × 1 mm) that were about 1 μm in thickness (Chart 2e). A section containing a single MWNT channel was then mounted on a support structure containing a hole, and this assembly was clamped between two chambers fabricated from polycarbonate and sealed with silicone O rings (Chart 2f). The inner diameter of the MWNT was measured by TEM (Chart 2g), and the channel length (or membrane thickness) was determined

Chart 2

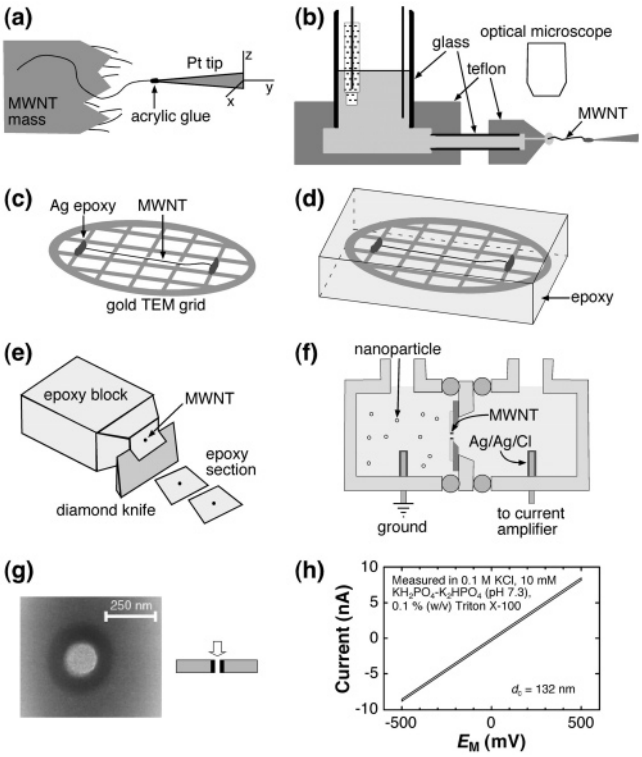

from the ionic conductance of the channel using cyclic voltammetry (Chart 2h).[1,2,26]

Fundamental Characteristics of CNCC Measurements. CNCC experiments were performed using the setup shown in Chart 2f. A solution containing polymeric nanoparticles was added to the chamber held at ground potential, and a particle-free solution was added to the other chamber. Buffer solutions containing KCl of relatively high concentration (0.1 M) were used to improve the signal-to-noise ratio. In addition, the surfactant Triton X-100 was added to the solutions to prevent the nanoparticles from aggregating and to ensure wetting of the hydrophobic MWNT channel.

Figure 1a shows a typical current-versus-time plot for an ensemble of nanoparticles having a low surface concentration of −COOH groups [low-surface-charged (LSC) nanoparticles: polystyrene, 57 ± 6 nm diameter, 120 −COOH/particle].[2] Current pulses (indicated by arrows) are observed when a positive membrane potential (+0.5 V) is applied, but no signal is observed when the membrane potential is either zero or negative. Moreover, parts b−d of Figure 1 indicate that the pulse width is larger at a lower potential. These two observations indicate that the nanoparticles are negatively charged and pass through the MWNT channel by electrophoresis. Nanoparticles having a higher surface concentration of −COOH groups [high-surface-charged (HSC) nanoparticles: copolymer of polystyrene−poly(acrylic acid), 60 ± 10 nm diameter, 24220 −COOH/particle] resulted in narrower pulse widths (Figure 1e), which is consistent with their higher surface charge and thus higher electrophoretic transport. Electroosmosis is negligible in these experiments, because

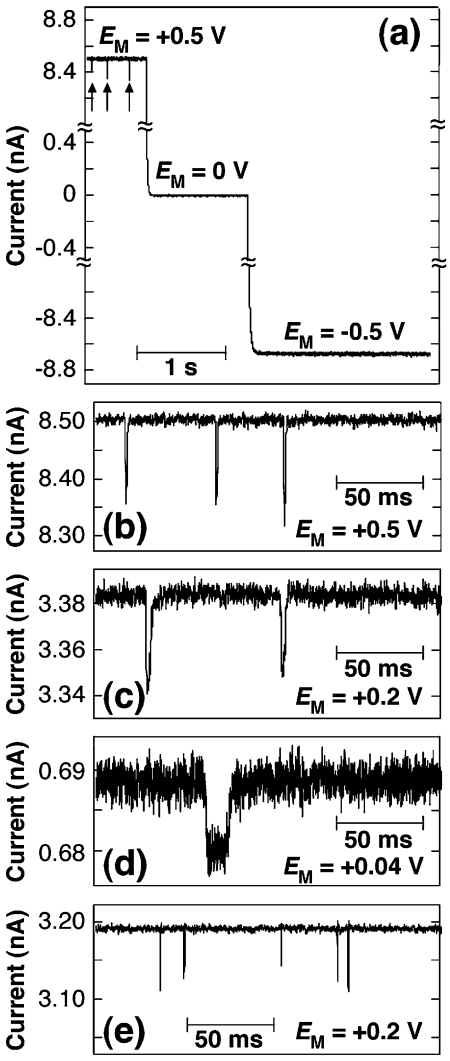

FIGURE 1. (a) Plot of current versus time for a single-component solution of LSC nanoparticles at three different membrane potentials. (b–d) High-resolution current-versus-time plots obtained for a solution containing LSC nanoparticles at the indicated values of E_M. (e) High-resolution current versus time plots obtained for a solution containing HSC nanoparticles at $E_M = +0.2$ V. These data were measured in solutions containing nominally 5×10^{11} particles/mL, 0.1 M KCl, 10 mM KH_2PO_4–K_2HPO_4 buffer (pH 7.3), and 0.1% (w/v) Triton X-100. The MWNT channel ($d_c = 132$ nm, $l_c = 939$ nm) was immobilized on a PDMS support.

streaming potential measurements indicate that the nanotube interiors support no measurable surface charge.[1]

Performance Improvement. According to eq 1, the diameter of each nanoparticle can be determined from the pulse height using data of the type shown in Figure 1. However, in our early work using Si/Si_3N_4 support structures (Chart 3a) true pulse heights could not be determined. For example, the measured diameter of 60-nm diameter particles (determined by TEM) was found by CNCC to be ~40 nm. This error is a consequence of signal distortion introduced by digital and analogue filtering, which was necessary because of the high noise level that arises from the relatively high capacitance of the Si/Si_3N_4 support.[27]

Chart 3

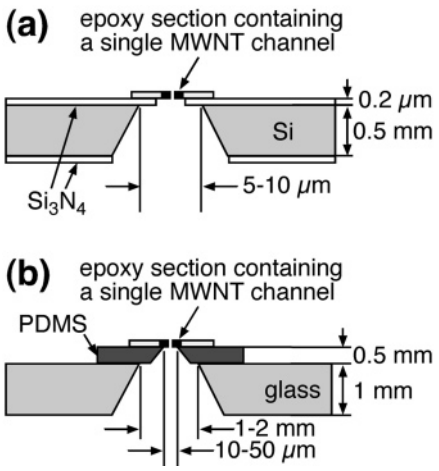

Reduction of the noise level can solve the types of problems described in the previous paragraph and also make it possible to obtain measurable signals from smaller particles. To address this issue, we replaced the Si/Si_3N_4 membrane support with a low-capacitance PDMS support structure.[2] PDMS is an insulator that is known to reduce electronic noise in patch-clamp experiments.[28] An additional advantage is that many PDMS support structures can be prepared using a simple molding process.[29] We found that the PDMS-based channel configuration (Chart 3b) results in more than a 20-fold reduction in the peak–peak noise, compared to the Si/Si_3N_4 support, which makes it possible to determine particle diameters as small as 28 nm. Additionally, noise reduction permits recording of current pulses using a relatively high cutoff frequency filter, which improves the time resolution of the CNCC from >1 ms to 50 μs.

Determination of Particle Size. Figure 2 shows the distribution of diameters, calculated using eq 1, for the LSC and HSC nanoparticles.[2] The results indicate that the diameter distributions are independent of the magnitude of the applied membrane potential, as anticipated by eq 1. Table 1 provides a comparison of particle diameters determined using three different techniques: CNCC, TEM, and dynamic light scattering (DLS).[3] Like TEM, CNCC measures many individual particles and thus yields the intrinsic distribution of sizes directly. It is satisfying to find that the CNCC yields size distributions consistent with TEM measurements (top half of Table 1). In contrast to CNCC and TEM, DLS only provides the average diameter directly; the size distribution can be obtained only indirectly by curve fitting.[30] At the bottom of Table 1, we have compared ensemble-averaged particle diameters obtained from many independent DLS measurements with the average diameter obtained using different CNCCs. The standard deviation in this case mainly reflects the reproducibility of sample preparation and measurements but not the true polydispersity of the nanoparticles. In summary, the above three techniques provide complementary information about particle size with some subtle differences (Chart 4): CNCC measures the size distribution based on the volume of the insulating portion of each

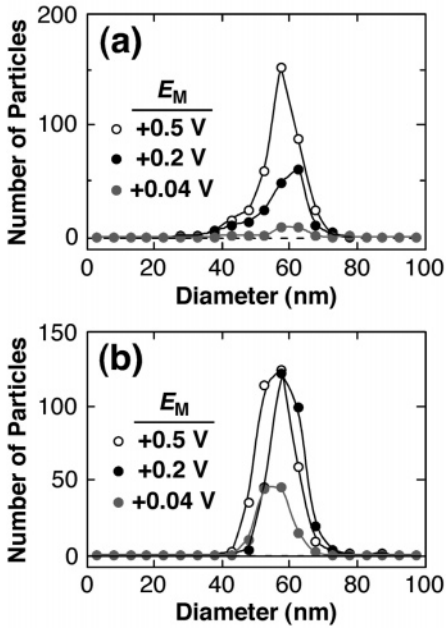

FIGURE 2. Distribution of the diameters of the (a) LSC and (b) HSC nanoparticles, calculated from signal-height data at $E_M = +0.5$, $+0.2$, and $+0.04$ V. Experimental conditions are the same as those in Figure 1. Note that the absolute number of counts in the distribution curves varies as a function of the total analysis time (see Tables 1 and 2 in ref 2).

Table 1. Measurements of Nanoparticle Diameters (Nanometers) Using CNCC, TEM, and DLS

Determined from Individual Particle Diameters[a]		
method	LSC nanoparticles	HSC nanoparticles
CNCC[b]	57 ± 8	59 ± 5
TEM (our results)	61 ± 9	57 ± 12
Determined from Averaged Diameters of Particle Ensemble[c]		
method	LSC nanoparticles	HSC nanoparticles
CNCC[d]	59 ± 2	58 ± 3
DLS[e]	57 ± 1	72 ± 1

[a] Values are the average and standard deviation obtained by measuring ensembles of particles. [b] Measured using a MWNT membrane.[2] [c] Values are the average and standard deviation of several separate ensemble measurements. [d] Calculated from the average diameters of 16−500 nanoparticles obtained using the 4 and 3 MWNT channels for the LSC and HSC nanoparticles, respectively. [e] Obtained using ≥5 measurements.

dispersed nanoparticle; TEM provides the size distribution of dry particles having collapsed surface structures; and DLS yields the average hydrodynamic size based on the diffusional velocity of the particle.[3] One such subtle difference can be illustrated by the data in Table 1, which was obtained using CNCC and DLS. For the LSC nanoparticles, the two techniques provide comparable results, but DLS yields a larger diameter for the HSC nanoparticles. This is a consequence of the origin of the signal from CNCC and DLS. Specifically, we rationalize this finding by assuming that the HSC nanoparticles consist of a solvent-swollen, highly charged layer atop a compact, insulating core. CNCC measures just the size of the insulating core, whereas DLS measures the hydrodynamic diameter of the entire, solvent-swollen particle (Chart 4a).

Chart 4

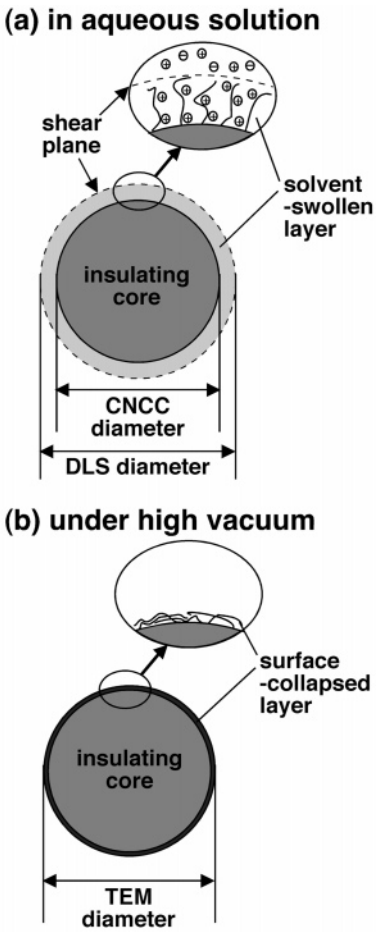

Determination of Electrophoretic Mobility and Surface Charge of Nanoparticles. Because MWNT channels are uncharged, they do not support mass transport by electroosmosis. This unique characteristic of CNCCs makes it possible to quantitatively relate the pulse width (Δt) to the surface charge (Q) of the analyte.[2] Specifically, in the case where the dominant mode of mass transport is electrophoresis, the average analyte velocity can be related to its electrophoretic mobility, μ, as shown in eq 4. Established theory (eq 5) links the electrophoretic

$$v_s = \frac{l_c'}{\Delta t} = \frac{\mu}{l_c'} E_M \tag{4}$$

mobility to the surface charge of a spherical particle. Here,

$$\mu = \frac{Q}{2\pi\eta d_s(1 + d_s/2d_D)} \tag{5}$$

d_D is the Debye length, which depends on the solution ionic strength. Equation 6 results from the combination of eqs 4 and 5. Equations 5 and 6 are based on two

$$Q = \frac{2\pi\eta l_c'^2 d_s(1 + d_s/2d_D)}{E_M \Delta t} \tag{6}$$

assumptions: the first is the Debye−Hückel approximation, which requires that the charge density (or the ζ

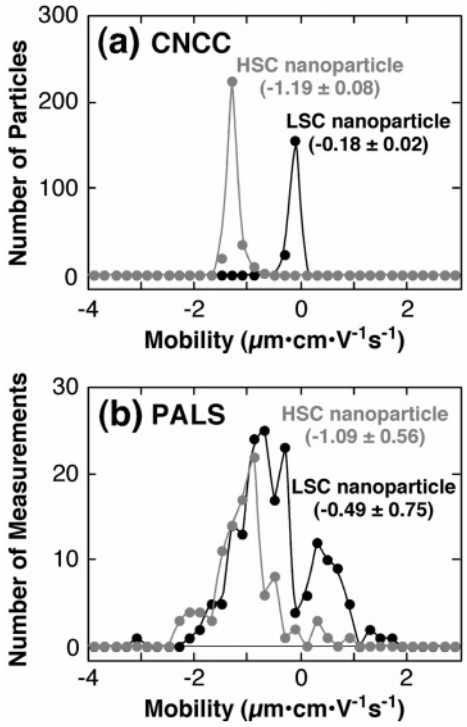

FIGURE 3. Distribution of electrophoretic mobilities for the LSC and HSC nanoparticles obtained using (a) a CNCC (d_c = 132 nm, l_c = 939 nm) and (b) PALS. Solution conditions are the same as those in Figure 1. The average and standard deviation of each measurement are also shown.

potential) of the particle is not too large, and the second is the Helmholz−Smoluchowski condition, which requires that the particle size be much larger than the Debye length.

Equation 4 shows that CNCCs are particularly well-suited for measuring very small particle mobilities, because the mobility is inversely proportional to the pulse width and longer pulse widths are easier to measure. This is a unique characteristic of CNCCs, because this type of information is accessible only for particles large enough to be individually observed under an optical/fluorescence microscope.[30,31] To illustrate this point, we next compare mobility measurements made using a CNCC and by using phase analysis light scattering (PALS).[3,30,31] PALS detects the frequency shift of scattered light (Doppler effect) caused by electrophoretically driven particle motion in an AC electric field, which can be converted to μ by curve fitting. The scattered light is derived from an ensemble of particles, and thus PALS provides only an ensemble-averaged value of particle mobility.

Figure 3 shows mobility data measured by CNCC and PALS for the LSC and HSC nanoparticles under identical solution conditions.[3] It is obvious that CNCC yields more precise results than PALS. The higher precision of the CNCC data probably arises from faster electrophoresis of the particles relative to Brownian diffusion, which is a consequence of the unique geometrical characteristics of the MWNT channel. Specifically, the short MWNT channel (~1 μm) makes it possible to achieve a large electric field

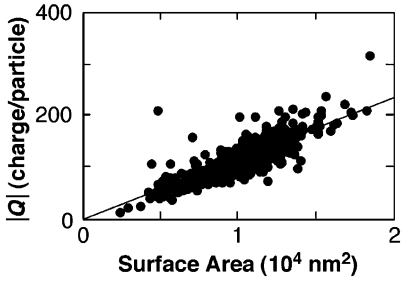

FIGURE 4. Total electrokinetic surface charge as a function of particle surface area for LSC nanoparticles. Experimental conditions are the same as those in Figure 1.

(~kV/cm) using a modest applied potential (<1 V). This results in fast electrophoretic transport of the particles. In contrast, the field strength used for PALS measurements (<10 V/cm) is so low that Brownian diffusion can cause a relatively large error. The large variation of the PALS data might also arise in part from contamination from electrochemical reactions occurring at the two driving electrodes. This suggests that the CNCC is more easily adapted for obtaining precise measurements for nanoparticles having low mobilities.[3]

Note that eq 6 is applicable to individual particles passing through the sensing channel, and thus CNCC provides a means for measuring the surface-charge-to-area ratio for individual particles within a nanoparticle ensemble. Figure 4 shows that this ratio is nearly constant for the LSC nanoparticles, even though there is substantial variation in the size of individual members of the ensemble. That is, even though the absolute size and charge vary, the surface properties of each particle are remarkably constant. The slope of the best-fit line through the data in Figure 4 is related to the average number of charges per unit surface area. The slope (0.011 charge/nm^2)[2] is very close to the number of −COOH groups per unit surface area (0.012 −COOH/nm^2) determined by the manufacturer, using conductometric titration. This result indicates that nearly all of the acid groups deprotonate under the conditions used to obtain the data shown in Figure 4.[2]

The same methods and conditions used to obtain the data in Figure 4 were also used to measure the charge density for the HSC nanoparticles. The measured value was found to be 830 ± 90 negative charges/particle, which is much smaller than 24 220 −COOH/particle determined by the manufacturer, using conductometric titration.[2] This discrepancy is likely caused by a combination of factors, such as the presence of a significant number of counter-cations within the hydrodynamic shear plane of the particles (Chart 4a) or break down of the Debye−Hückel approximation.[30] The former point is probably very important, because the surface charge measured by the CNCCs is really an electrokinetic charge, which is the sum of charges contributed from all species located within the hydrodynamic shear plane of the particle.

To summarize, the CNCC is a promising device for precisely measuring low-magnitude mobility or charge of individual nanoparticles in aqueous solution. The technique also offers an opportunity to correlate size and

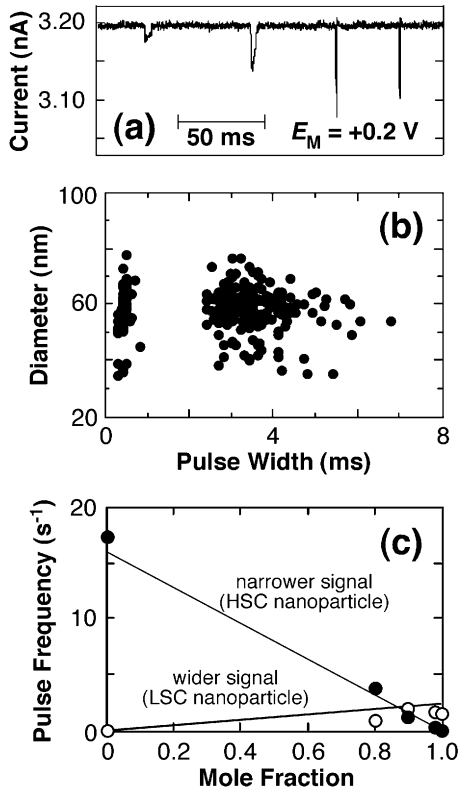

FIGURE 5. (a) Plot of current versus time obtained for a mixed solution of LSC and HSC nanoparticles present at a molar ratio of 4:1. (b) Relationship between particle diameter and pulse width obtained for the mixed solution of LSC and HSC nanoparticles. (c) Relationship between pulse frequency and mole fraction for LSC nanoparticles. The solid lines were calculated using the average particle diameter and surface charge, determined from CNCC measurements, and the nominal total particle concentration. Experimental conditions are the same as those in Figure 1, except the total particle concentration (5×10^{11} particles/mL for LSC and HSC nanoparticles). $E_M = +0.2$ V.

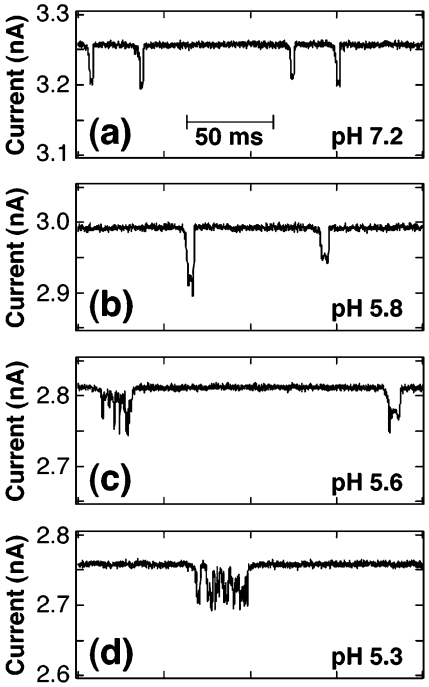

FIGURE 6. High-resolution plots of current versus time obtained using LSC nanoparticle solutions at the indicated pHs. All data were measured in solutions containing nominally 5×10^{11} LSC nanoparticles/mL, 0.1 M KCl, 10 mM KH_2PO_4–K_2HPO_4 buffer, and 0.1% (w/v) Triton X-100. The MWNT channel ($d_c = 132$ nm, $l_c = 955$ nm) was immobilized on a PDMS support. $E_M = +0.2$ V. The time axis is the same for each frame of the figure.

charge data for individual nanoparticles within a large ensemble.

Differentiation of Polymeric Nanoparticles Based on Their Size and Surface Charge. The feasibility of making simultaneous size and charge measurements using CNCCs provides a basis for differentiating between the components of a mixture of particles when each component has a unique combination of size and charge.[2] Figure 5a shows a typical current-versus-time plot for a solution containing a mixture of LSC and HSC nanoparticles present at a molar ratio of 4:1. Two distinct types of current pulses are observed: the wider pulses correspond to LSC nanoparticles, and the narrower ones correspond to HSC nanoparticles. Figure 5b shows all of the pulse signals plotted in a two-dimensional (diameter and pulse width) parameter space;[14] it is clear that the two types of particles can be clearly distinguished in this data set. Because two types of nanoparticles are distinguishable in Figure 5b, it is possible to independently determine their concentrations from their respective pulse frequencies. Indeed, Figure 5c shows that plots of pulse frequency for the two types of nanoparticles lie on theoretical lines calculated using the average particle diameter and surface charge, determined from CNCC measurements, and the nominal total particle concentration (5×10^{11} particles/mL).[2]

Determination of the Apparent Surface pK_a of Charged Nanoparticles. It is possible to use a CNCC to determine the apparent surface pK_a of nanoparticles by measuring the surface charge as a function of pH. Figure 6 shows CNCC current-versus-time plots for the LSC nanoparticles at four different pHs. Well-defined pulse signals, corresponding to single-particle transport events, are observed between pH 7.2 and 5.8, but note that the pulse width increases with decreasing pH. This is a consequence of pH-dependent surface charge of these acid-functionalized particles. At pH 5.6, current pulses composed of multiple peaks are occasionally observed (Figure 6c), and these features become more common as the pH is further decreased (Figure 6d). Because the height (Δi_c) of the multiple-peak pulses is very similar to the height for typical single-peak pulses, they cannot be attributed to aggregates of particles, which would act as large single particles and thus yield higher pulse heights. Indeed, the average particle diameters, measured by both DLC and CNCC (Figure 7a), are very similar (52–64 nm) over the entire pH range studied. At present, we believe that slow mass transport at low pH results in occasional reversible attachment of particles around the entrance or at the inner wall of the sensing channel. Confirmation of this hypothesis awaits additional experiments, however.

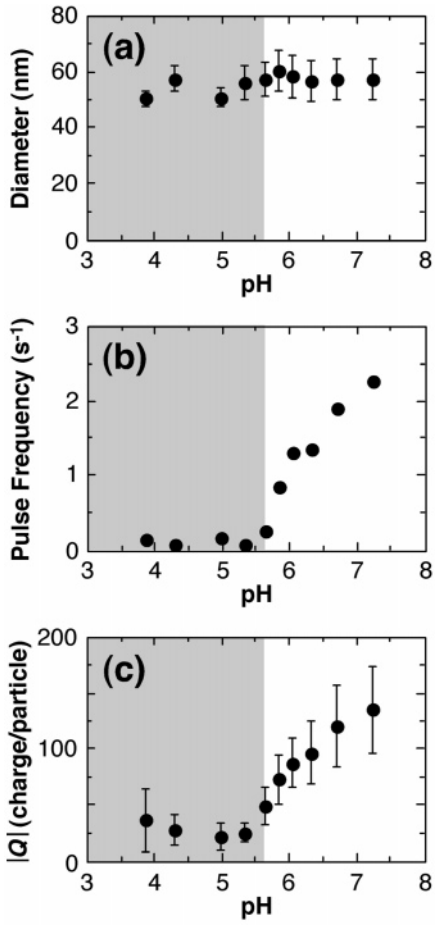

FIGURE 7. Effect of pH on the (a) diameter, (b) pulse frequency, and (c) surface charge of LSC nanoparticles measured using a CNCC. In a and c, the plots and error bars indicate the averages and standard deviations measured using individual particle data. Experimental conditions are the same as those indicated in Figure 6.

Figure 7 provides CNCC-measured nanoparticle diameters, the pulse frequency, and surface charge between pH 7.2 and 3.9. Although multiple-peak pulses are observed at pH < 5.6 (the shaded range in Figure 7), the average particle diameter remains constant throughout the entire pH range. However, both the pulse frequency and surface charge increase significantly at pH > 5.6. Other experiments, carried out using a different nanotube channel, showed that the surface charge remained constant between pH 7.2 and 9.0, indicating that most of the surface −COOH groups are deprotonated at pH > 7.2. Thus, Figure 7c indicates that the apparent surface pK_a, defined as the pH where the surface charge attains half of its maximum value, is ∼5.8. This value is similar to that determined using pH titration for polystyrene particles (∼300 nm in diameter) having a higher surface −COOH density (5.7−5.8).[32] Note, however, that the pH titration requires purified nanoparticle solutions, because the presence of small-molecule acids or bases affect the results.[33,34] In contrast, CNCC results are not affected by such contaminants. Additionally, more dilute nanoparticle solutions can be used for CNCC measurements than in conventional titrations.[34]

Summary, Conclusions, and Outlook

This Account has described the properties of CNCCs and some of their applications. The unique characteristics of CNCCs originate from the smooth and uniform cylindrical structure of MWNTs, its high level of stability, the absence of permanent charge on its interior surface, and the high electric field present across the short channel. CNCCs provide a means for simultaneously determining the size and electrophoretic mobility (or electrokinetic surface charge) of single nanoparticles from signal height and width measurements, respectively.[2] Such measurements do not require calibration of the CNCC, nor do they require analyte labeling. Moreover, because CNCCs measure the properties of individual particles, they provide true average and polydispersity distributions. The CNCC method provides information that is complementary to that available from TEM and DLS, and it can be used to determine the electrophoretic mobilities of dispersed particles more precisely than light-scattering techniques such as PALS.[3]

In addition to its strengths, CNCCs have some weaknesses. For example, CNCCs can only detect particles within a particular size range (∼28−90 nm in diameter for a MWNT channel that is 132 nm in diameter) and normally require a relatively high concentration of supporting electrolyte. However, CNCCs having different channel diameters can be chosen according to the size of analytes, and the requirement of high electrolyte concentration is suitable for measurements under physiological conditions. MWNT channels can become blocked by aggregated or adventitious particles, which may limit the lifetime of a CNCC to a few hours. However, we believe this problem can be solved by controlling the surface properties of the MWNT channels.

We anticipate that CNCCs will be useful for studying the properties of colloids and for better understanding mass transport in nanoporous media. Furthermore, we believe CNCCs will be useful for detection and characterization of biological materials such as viruses, proteins, and DNA under physiological conditions. Our present efforts are directed toward these targets. It may also be possible to use CNCCs to better understand biological and chemical reactions.

We gratefully acknowledge financial support from the U.S. Department of Energy (Contract no. DE-FG03-01ER15247). We thank Dr. Michael A. Bevan (Department of Chemical Engineering, Texas A&M University) for generous help in DLS and PALS measurements; Dr. Henry S. White (University of Utah) for insightful discussions on quantitative analysis of transport problems; Drs. Hagan Bayley, Orit Braha, LiQun Gu, and William Lackowski (Department of Chemistry, Texas A&M University) for their helpful suggestions; Drs. Helga Sittertz-Bhatkar, Zhiping Luo, and E. Ann Ellis (Microscopy and Imaging Center, Texas A&M University) for their assistance with microtoming and TEM imaging; Dr. D. G. Glasgow (Applied Sciences, Inc., Cedarville, OH) for providing the carbon nanotubes used in this study; and Kevin Roberts (University of Minnesota) for assistance with silicon etching.

References

(1) Sun, L.; Crooks, R. M. Single Carbon Nanotube Membranes: A Well-Defined Model for Studying Mass Transport through Nanoporous Materials. *J. Am. Chem. Soc.* **2000**, *122*, 12340−12345.

(2) Ito, T.; Sun, L.; Crooks, R. M. Simultaneous Determination of the Size and Surface Charge of Individual Nanoparticles Using a Carbon Nanotube-Based Coulter Counter. *Anal. Chem.* **2003**, *75*, 2399−2406.

(3) Ito, T.; Sun, L.; Bevan, M. A.; Crooks, R. M. Comparison of Nanoparticle Size and Electrophoretic Mobility Measurements Using a Carbon Nanotube-Based Coulter Counter, Dynamic Light Scattering, Transmission Electron Microscopy, and Phase Analysis Light Scattering. *Langmuir* **2004**, *20*, 6940−6945.

(4) Coulter, W. H. U.S. Patent 2,656,508, October 20, 1953.

(5) Williams, W. J.; Beutler, E.; Erslev, A. J.; Lichtman, M. A. *Hematology*; 3rd ed.; McGraw−Hill: New York, 1983.

(6) DeBlois, R. W.; Bean, C. P. Counting and Sizing of Submicron Particles by the Resistive Pulse Technique. *Rev. Sci. Instrum.* **1970**, *41*, 909−916.

(7) DeBlois, R. W.; Wesley, R. K. A. Sizes and Concentrations of Several Type C Oncornaviruses and Bacteriophage T2 by the Resistive-Pulse Technique. *J. Virol.* **1977**, *23*, 227−233.

(8) DeBlois, R. W.; Uzgiris, E. E.; Cluxton, D. H.; Mazzone, H. M. Comparative Measurements of Size and Polydispersity of Several Insect Viruses. *Anal. Biochem.* **1978**, *90*, 273−288.

(9) Li, J.; Stein, D.; McMullan, C.; Branton, D.; Aziz, M. J.; Golovchenko, J. A. Ion-Beam Sculpting at Nanometre Length Scales. *Nature* **2001**, *412*, 166−169.

(10) Li, J.; Gershow, M.; Stein, D.; Brandin, E.; Golovchenko, J. A. DNA Molecules and Configurations in a Solid-State Nanopore Microscope. *Nat. Mater.* **2003**, *2*, 611−615.

(11) Mara, A.; Siwy, Z.; Trautmann, C.; Wan, J.; Kamme, F. An Asymmetric Polymer Nanopore for Single Molecule Detection. *Nano Lett.* **2004**, *4*, 497−501.

(12) Kasianowicz, J. J.; Brandin, E.; Branton, D.; Deamer, D. W. Characterization of Individual Polynucleotide Molecules Using a Membrane Channel. *Proc. Natl. Acad. Sci. U.S.A.* **1996**, *93*, 13770−13773.

(13) Bayley, H.; Martin, C. R. Resistive-Pulse Sensing—From Microbes to Molecules. *Chem. Rev.* **2000**, *100*, 2575−2594.

(14) Deamer, D. W.; Branton, D. Characterization of Nucleic Acids by Nanopore Analysis. *Acc. Chem. Res.* **2002**, *35*, 817−825.

(15) Saleh, O. A.; Sohn, L. L. Quantitative Sensing of Nanoscale Colloids Using a Microchip Coulter Counter. *Rev. Sci. Instrum.* **2001**, *72*, 4449−4451.

(16) Saleh, O. A.; Sohn, L. L. An Artificial Nanopore for Molecular Sensing. *Nano Lett.* **2003**, *3*, 37−38.

(17) Saleh, O. A.; Sohn, L. L. Direct Detection of Antibody−Antigen Binding Using an On-Chip Artificial Pore. *Proc. Natl. Acad. Sci. U.S.A.* **2003**, *100*, 820−824.

(18) Henriquez, R. R.; Ito, T.; Sun, L.; Crooks, R. M. The Resurgence of Coulter Counting for Analyzing Nanoscale Objects. *Analyst* **2004**, *129*, 478−482.

(19) Lines, R. W. In *Particle Size Analysis*; Stanley-Wood, N. G., Linew, R. W., Eds.; Royal Society of Chemistry: Cambridge, U.K.,1992; pp 351−383.

(20) Scott, E. R.; White, H. S.; Phipps, J. B. Scanning Electrochemical Microscopy of a Porous Membrane. *J. Membr. Sci.* **1991**, *58*, 71−87.

(21) In our previous publications (see refs 1 and 18), we used an approximate equation that assumes the four transport modes are independent of each other. This approximation may lead to large numeric errors under some conditions, however, and therefore, it should be used with great care.

(22) Bezrukov, S. M. Ion Channels as Molecular Coulter Counters to Probe Metabolite Transport. *J. Membr. Biol.* **2000**, *174*, 1−13.

(23) Harris, P. J. F. *Carbon Nanotubes and Related Structures*; Cambridge University Press: Cambridge, U.K., 1999.

(24) Campbell, J. K.; Sun, L.; Crooks, R. M. Electrochemistry Using Single Carbon Nanotubes. *J. Am. Chem. Soc.* **1999**, *121*, 3779−3780.

(25) Ito, T.; Sun, L.; Crooks, R. M. Electrochemical Etching of Individual Multiwall Carbon Nanotubes. *Electrochem. Solid-State Lett.* **2003**, *6*, C4−C7.

(26) Ito, T.; Sun, L.; Crooks, R. M. Observation of DNA Transport through a Single Carbon Nanotube Channel Using Fluorescence Microscopy. *Chem. Commun.* **2003**, 1482−1483.

(27) Sun, L.; Crooks, R. M. Fabrication and Characterization of Single Pores for Modeling Mass Transport across Porous Membranes. *Langmuir* **1999**, *15*, 738−741.

(28) Levis, R. A.; Rae, J. L. Low-Noise Patch-Clamp Techniques. *Methods Enzymol.* **1998**, *293*, 218−266.

(29) Klemic, K. G.; Klemic, J. F.; Reed, M. A.; Sigworth, F. J. Micromolded PDMS Planar Electrode Allows Patch Clamp Electrical Recordings from Cells. *Biosens. Bioelectron.* **2002**, *17*, 597−604.

(30) Hunter, R. J. *Foundations of Colloid Science*; Oxford University Press: New York, 2001.

(31) Delgado, A. V.; Arroyo, F. J. In *Interfacial Electrokinetics and Electrophoresis*; Delgado, A. V., Ed.; Marcel Dekker: New York, 2002; pp 1−54.

(32) Bastos-González, D.; Ortega-Vinuesa, J. L.; De Las Nieves, F. J.; Hidalgo-Álvarez, R. Carboxylated Latexes for Covalent Coupling Antibodies, I. *J. Colloid Interface Sci.* **1995**, *176*, 232−239.

(33) Vanderhoff, J. W.; Van den Hul, H. J.; Tausk, R. J. M.; Overbeek, J. T. G. In *Clean Surfaces: Their Preparation and Characterization for Interfacial Studies*; Goldfinger, G., Ed.; Marcel Dekker: New York, 1970; pp 15−44.

(34) Ito, T.; Sun, L.; Crooks, R. M. Unpublished results.

AR040108+